CLEO CONF 98-22
ICHEP98 1012

Search for Electroweak Penguin Decays $B \to K l^+ l^-$ and $B \to K^* l^+ l^-$ at CLEO

CLEO Collaboration

(July 22, 1998)

Abstract

CLEO has searched for the electroweak penguin decays of B mesons to final states with a K or K^* and two oppositely charged leptons. Using a data sample of 3.33×10^6 produced $B\bar{B}$ events, no signal is observed in any of the 12 final states studied. The branching fraction upper limits for the $\mu^+\mu^-$ and e^+e^- samples combined are $\mathcal{B}(B \to l^+l^-K) < 0.70 \times 10^{-5}$ and $\mathcal{B}(B \to l^+l^-K^*) < 0.68 \times 10^{-5}$ (for $m_{ll} > 0.5$ GeV/c^2) at 90% confidence level. Upper limits on branching fractions for the individual $\mu^+\mu^-$ and e^+e^- modes are also obtained. Among these upper limits the $K^{*0}e^+e^-$ result of $\mathcal{B}(B \to e^+e^-K^{*0}) < 1.3 \times 10^{-5}$ at 90% confidence level is the closest to the predicted range in the Standard Model.

R. Godang,[1] K. Kinoshita,[1] I. C. Lai,[1] P. Pomianowski,[1] S. Schrenk,[1] G. Bonvicini,[2] D. Cinabro,[2] R. Greene,[2] L. P. Perera,[2] G. J. Zhou,[2] S. Chan,[3] G. Eigen,[3] E. Lipeles,[3] J. S. Miller,[3] M. Schmidtler,[3] A. Shapiro,[3] W. M. Sun,[3] J. Urheim,[3] A. J. Weinstein,[3] F. Würthwein,[3] D. E. Jaffe,[4] G. Masek,[4] H. P. Paar,[4] E. M. Potter,[4] S. Prell,[4] V. Sharma,[4] D. M. Asner,[5] J. Gronberg,[5] T. S. Hill,[5] D. J. Lange,[5] R. J. Morrison,[5] H. N. Nelson,[5] T. K. Nelson,[5] D. Roberts,[5] B. H. Behrens,[6] W. T. Ford,[6] A. Gritsan,[6] H. Krieg,[6] J. Roy,[6] J. G. Smith,[6] J. P. Alexander,[7] R. Baker,[7] C. Bebek,[7] B. E. Berger,[7] K. Berkelman,[7] V. Boisvert,[7] D. G. Cassel,[7] D. S. Crowcroft,[7] M. Dickson,[7] S. von Dombrowski,[7] P. S. Drell,[7] K. M. Ecklund,[7] R. Ehrlich,[7] A. D. Foland,[7] P. Gaidarev,[7] R. S. Galik,[7] L. Gibbons,[7] B. Gittelman,[7] S. W. Gray,[7] D. L. Hartill,[7] B. K. Heltsley,[7] P. I. Hopman,[7] J. Kandaswamy,[7] D. L. Kreinick,[7] T. Lee,[7] Y. Liu,[7] N. B. Mistry,[7] C. R. Ng,[7] E. Nordberg,[7] M. Ogg,[7,*] J. R. Patterson,[7] D. Peterson,[7] D. Riley,[7] A. Soffer,[7] B. Valant-Spaight,[7] A. Warburton,[7] C. Ward,[7] M. Athanas,[8] P. Avery,[8] C. D. Jones,[8] M. Lohner,[8] C. Prescott,[8] A. I. Rubiera,[8] J. Yelton,[8] J. Zheng,[8] G. Brandenburg,[9] R. A. Briere,[9] A. Ershov,[9] Y. S. Gao,[9] D. Y.-J. Kim,[9] R. Wilson,[9] H. Yamamoto,[9] T. E. Browder,[10] Y. Li,[10] J. L. Rodriguez,[10] S. K. Sahu,[10] T. Bergfeld,[11] B. I. Eisenstein,[11] J. Ernst,[11] G. E. Gladding,[11] G. D. Gollin,[11] R. M. Hans,[11] E. Johnson,[11] I. Karliner,[11] M. A. Marsh,[11] M. Palmer,[11] M. Selen,[11] J. J. Thaler,[11] K. W. Edwards,[12] A. Bellerive,[13] R. Janicek,[13] P. M. Patel,[13] A. J. Sadoff,[14] R. Ammar,[15] P. Baringer,[15] A. Bean,[15] D. Besson,[15] D. Coppage,[15] C. Darling,[15] R. Davis,[15] S. Kotov,[15] I. Kravchenko,[15] N. Kwak,[15] L. Zhou,[15] S. Anderson,[16] Y. Kubota,[16] S. J. Lee,[16] R. Mahapatra,[16] J. J. O'Neill,[16] R. Poling,[16] T. Riehle,[16] A. Smith,[16] M. S. Alam,[17] S. B. Athar,[17] Z. Ling,[17] A. H. Mahmood,[17] S. Timm,[17] F. Wappler,[17] A. Anastassov,[18] J. E. Duboscq,[18] K. K. Gan,[18] T. Hart,[18] K. Honscheid,[18] H. Kagan,[18] R. Kass,[18] J. Lee,[18] H. Schwarthoff,[18] A. Wolf,[18] M. M. Zoeller,[18] S. J. Richichi,[19] H. Severini,[19] P. Skubic,[19] A. Undrus,[19] M. Bishai,[20] S. Chen,[20] J. Fast,[20] J. W. Hinson,[20] N. Menon,[20] D. H. Miller,[20] E. I. Shibata,[20] I. P. J. Shipsey,[20] S. Glenn,[21] Y. Kwon,[21,†] A.L. Lyon,[21] S. Roberts,[21] E. H. Thorndike,[21] C. P. Jessop,[22] K. Lingel,[22] H. Marsiske,[22] M. L. Perl,[22] V. Savinov,[22] D. Ugolini,[22] X. Zhou,[22] T. E. Coan,[23] V. Fadeyev,[23] I. Korolkov,[23] Y. Maravin,[23] I. Narsky,[23] R. Stroynowski,[23] J. Ye,[23] T. Wlodek,[23] M. Artuso,[24] E. Dambasuren,[24] S. Kopp,[24] G. C. Moneti,[24] R. Mountain,[24] S. Schuh,[24] T. Skwarnicki,[24] S. Stone,[24] A. Titov,[24] G. Viehhauser,[24] J.C. Wang,[24] J. Bartelt,[25] S. E. Csorna,[25] K. W. McLean,[25] S. Marka,[25] and Z. Xu[25]

[1]Virginia Polytechnic Institute and State University, Blacksburg, Virginia 24061
[2]Wayne State University, Detroit, Michigan 48202
[3]California Institute of Technology, Pasadena, California 91125
[4]University of California, San Diego, La Jolla, California 92093
[5]University of California, Santa Barbara, California 93106
[6]University of Colorado, Boulder, Colorado 80309-0390

[*]Permanent address: University of Texas, Austin TX 78712.

[†]Permanent address: Yonsei University, Seoul 120-749, Korea.

[7]Cornell University, Ithaca, New York 14853
[8]University of Florida, Gainesville, Florida 32611
[9]Harvard University, Cambridge, Massachusetts 02138
[10]University of Hawaii at Manoa, Honolulu, Hawaii 96822
[11]University of Illinois, Urbana-Champaign, Illinois 61801
[12]Carleton University, Ottawa, Ontario, Canada K1S 5B6
and the Institute of Particle Physics, Canada
[13]McGill University, Montréal, Québec, Canada H3A 2T8
and the Institute of Particle Physics, Canada
[14]Ithaca College, Ithaca, New York 14850
[15]University of Kansas, Lawrence, Kansas 66045
[16]University of Minnesota, Minneapolis, Minnesota 55455
[17]State University of New York at Albany, Albany, New York 12222
[18]Ohio State University, Columbus, Ohio 43210
[19]University of Oklahoma, Norman, Oklahoma 73019
[20]Purdue University, West Lafayette, Indiana 47907
[21]University of Rochester, Rochester, New York 14627
[22]Stanford Linear Accelerator Center, Stanford University, Stanford, California 94309
[23]Southern Methodist University, Dallas, Texas 75275
[24]Syracuse University, Syracuse, New York 13244
[25]Vanderbilt University, Nashville, Tennessee 37235

I. INTRODUCTION

Flavor changing neutral current (FCNC) processes are forbidden in the Standard Model (SM) at tree level. They can, however, occur via higher order processes such as box diagrams or penguin loops, yielding suppressed rates in the SM. Therefore, these processes are sensitive to non-SM physics since heavy particles such as charged Higgs bosons [1] [2], new gauge bosons, and supersymmetric particles [3], as well as anomalous trilinear gauge couplings [4] can contribute via additional loop or box diagrams. Previously, CLEO has observed such a process: evidence for the electromagnetic penguin decay $b \to s\gamma$ was found both in the exclusive $K^*\gamma$ final states [14] and in the inclusive photon energy spectrum [15].

Other FCNC processes, that are both experimentally [17] [18] and theoretically [6] of great interest, are the electroweak penguin decays $b \to sl^+l^-$. The lowest order SM diagrams are shown in Figure 1. Since higher order QCD corrections are expected to be lower here than in $b \to s\gamma$ [7], these modes are well-suited for testing the SM. Rates predicted in the SM, however, are suppressed by nearly two orders of magnitude with respect to those in the radiative channels. A detailed study of the properties of the 3-body decay, such as the dilepton invariant mass and the helicity angle of one lepton in the dilepton rest frame provide additional detailed tests of the SM [8] [10].

In the SM the effective Hamiltonian for the electroweak $B \to X_s l^+l^-$ penguin processes is parametrized by a sum of 3 local 4-quark operators multiplied by Wilson coefficient functions [5]. The 4-quark operators are the magnetic penguin operator Q_7, which describes $b \to s\gamma$, and two semileptonic operators Q_9 and Q_{10}. The Wilson coefficient functions $C_7(\mu), C_9(\mu)$ and $C_{10}(\mu)$ characterize the Cabibbo-Kobayashi-Maskawa (CKM) matrix elements of the process and the perturbative QCD effects, while the non-perturbative QCD effects are put into the hadronic matrix element. There are two scales involved, the weak scale occuring at short distances and the hadronization scale occuring at long distances, which is reflected in the Wilson coefficient functions. Due to renormalization, C_7 and C_9 acquire contributions from other operators. It is customary to define effective Wilson coefficient functions $C_7^{(0)eff}(\mu)$ and $C_9^{eff}(\mu)$. New physics can give contributions to any of the three Wilson coefficient functions.

Some SM predictions are listed in Table I. These models can be grouped into those which determine form factors (Greub-Wyler [10], Ball-Braun [11], Melikhov-Nikitin) [12] and those which use the heavy quark limit (Ali-Mannel) [7]. The determination of the form factor is performed using the light cone quark model in the Greub-Wyler model, a light cone sum rule approach in the Ball-Braun model, and the constituent quark model in the Melikhov-Nikitin model. Ali-Mannel use two different universal functions to calculate branching fractions: an exponential form (I) and a monopole form (II). The predictions are based on the following inputs: $\mid V_{ts} \mid = 0.039$, B lifetime $\tau_B = 1.6$ ps, a renormalization scale $\mu = m_b$ and a running top quark mass of $\bar{m}_t = 167$ GeV/c^2. The predictions of Melikhov-Nikitin were taken from reference [12] and rescaled with $\mid V_{ts} \mid = 0.039$. For all the other models $C_9^{eff}(\mu)$ is determined in next-to-leading order in the NDR scheme. [13] While the inclusive $B \to X_s l^+l^-$ rates are rather well predicted [9], branching fractions for exclusive modes studied here carry a larger theoretical uncertainty due to long distance effects involved in the hadronization. This is reflected in the spread of theoretical predictions listed in Table I.

Recently, CLEO reported on a search for the inclusive $B \to X_s l^+l^-$ modes [16]. We

TABLE I. Branching Fraction Predictions in the Standard Model for $B \to K^{(*)} l^+ l^-$ decays

mode	Greub-Wyler [10] $[10^{-6}]$	Ball-Braun [11] $[10^{-6}]$	Ali-Mannel I [7] $[10^{-6}]$	Ali-Mannel II [7] $[10^{-6}]$	Melikhov-Nikitin [12] $[10^{-6}]$
$\mu^+\mu^- K$	0.33 ± 0.07	0.51 ± 0.1	0.26 ± 0.1	0.69 ± 0.25	0.59 ± 0.12
$\mu^+\mu^- K^*$	1.0 ± 0.2	1.7 ± 0.3	2.5 ± 1.0	3.0 ± 1.2	1.4 ± 0.5
$e^+e^- K$	0.33 ± 0.07	0.51 ± 0.1	0.26 ± 0.1	0.69 ± 0.25	0.59 ± 0.12
$e^+e^- K^*$	1.4 ± 0.3	2.3 ± 0.5	3.7 ± 1.4	4.3 ± 1.7	1.8 ± 0.6

present herein results of a search for exclusive B decays to a K or a K^* recoiling against a pair of muons or electrons. A total of 12 exclusive final states has been studied.

II. DATA SELECTION

The data were collected with the CLEO II detector at the Cornell Electron Storage Ring (CESR). They consist of a luminosity of 3.15 fb^{-1} accumulated on the $\Upsilon(4S)$ resonance and of 1.64 fb^{-1} taken in the continuum 60 MeV below the $\Upsilon(4S)$ mass peak. This corresponds to 3.33×10^6 produced $B\bar{B}$ events. The CLEO II detector, described in detail elsewhere, [19] is a universal multipurpose magnetic detector with good momentum measurement over 95% of the solid angle, good electromagnetic energy measurements over 98% of the solid angle and good muon identification.

From the standard CLEO hadronic event sample we select candidates with at least four good-quality charged tracks originating from the primary vertex ($\Delta r \leq 0.5$cm, $\mid \Delta$z $\mid\leq 5$cm). Two of these tracks have to be leptons, either e^+e^- or $\mu^+\mu^-$. Electrons are identified in the standard way using the ionization loss in the drift chamber and the ratio of observed electromagnetic energy in the calorimeter and the momentum. To reduce the misidentification rate we require that one of electrons have a minimal momentum of 0.6 GeV/c, and the other a minimal momentum of 1.3 GeV/c. Muons are identified by requiring a minimal momentum of 1 GeV/c and a penetration of at least 3 interaction lengths in the iron. To reduce background from pion feed-through we require that at least one of the muons penetrate more than 5 interaction lengths of iron. For pion and kaon identification we just require a 3σ consistency from both the ionization measurements in the drift chamber and the time-of-flight measurements.

Photons are selected from isolated neutral showers whose profiles are consistent with that of an electromagnetic shower [20] and have a minimum energy of 0.04 (0.06) GeV in the barrel (endcap) electromagnetic calorimeters. To select π^0 candidates, one of the photons must have an energy greater 0.08 GeV and the $\gamma\gamma$ invariant mass must lie in the region $\mid m_{\gamma\gamma} - M_{\pi^0} \mid \leq 0.015$ GeV/c^2. K^0_S mesons are reconstructed in the $\pi^+\pi^-$ final state, requiring an invariant mass of $\mid m_{\pi^+\pi^-} - M_{K^0_S} \mid \leq 0.013$ GeV/c^2. The reconstruction of K^{*0}'s (K^{*+}'s) is performed in the $K^+\pi^-(K^+\pi^0)$ and $K^0_S\pi^0(K^0_S\pi^+)$ decays. The K^* candidates are selected by requiring that the $K\pi$ invariant mass lie within 0.1 GeV/c^2 of the nominal K^* mass.

The dileptons and candidate hadrons are combined to form a B meson candidate. Since the $\Upsilon(4S)$ resonance lies below the $B\bar{B}\pi$ threshold, all B mesons carry the beam energy and have a fixed momentum of ~ 300 MeV/c. We utilize these constraints by requiring an energy difference of the observed energy and the beam energy $\Delta E = \sum_i E_i - E_{beam}$ close to zero, and a beam-constrained mass $M_B = \sqrt{E_{beam}^2 - (\sum_i \vec{p}_i)^2}$ close to the nominal B meson mass, where E_i and p_i are energy and momentum of the i^{th} daughter of the B candidate.

To suppress $q\bar{q}$ continuum background we have constructed a Fisher discriminant based on four variables: the thrust of the B candidate, the sphericity of the B candidate, the angle between the thrust axis of the B candidate and that of the rest of the event and the polar angle of the B direction in the lab frame. A Fisher discriminant is a linear polynomial in the input variables. The coefficients are optimized to obtain the best separation of the signal and the background Monte Carlo sample in the distribution of the Fisher discriminant.

Since the dilepton mass spectra differ for the $B \to K^{(*)} l^+ l^-$ modes we have defined three separate Fisher discriminants: one for all $K l^+ l^-$ modes, one for all $K^* \mu^+ \mu^-$ modes and one for all $K^* e^+ e^-$ modes. We have used signal and $q\bar{q}$ Monte Carlo samples to determine the Fisher discriminant coefficients. The resulting distributions for signal and $q\bar{q}$ background are shown in Figure 2. As a cross check the Fisher discriminant distributions from off-resonance data are shown overplotted. They are in good agreement with those obtained from the $q\bar{q}$ continuum Monte Carlo. The shapes of Fisher discriminants for the three signal modes are rather similar.

To optimize the separation between signal and background we have studied the efficiency versus square root of background as a function of the Fisher discriminant. The optimization is done mode-by-mode and yields constraints on the Fisher discriminants of $F < 0.6 - 0.68$.

Further continuum background reduction is achieved by constraining the ratio of second-to-zeroth Fox-Wolfram moments to $R_2 < 0.4$, except for $K^+\pi^0$ final states where the constraint is tightened to $R_2 < 0.35$.

Since one of the main backgrounds involves modes with neutrinos we further impose mode-dependent requirements on the ratio of visible energy in the detector to the total energy. We again optimize the ratio of efficiency to square root of background mode-by-mode. The resulting ranges are $0.7 - 0.8 < E_{obs}/E_{tot} < 1.1$.

In order to prevent multiple entries per event we define a χ^2 distribution for each mode based on the difference of observed energy and beam energy ΔE, pion/kaon weights determined from dE/dx energy loss and TOF measurements and intermediate resonance massses, such as π^0, K^{*0} and K^{*+}:

$$\chi^2 = \left(\frac{\Delta E}{\sigma_{\Delta E}}\right)^2 + \sum_{i=1}^{n} W_i^2(dE/dx) + \sum_{i=1}^{n} W_i^2(TOF) + \sum_{i=1}^{N_{res}} \frac{(m_i - m_i^{res})^2}{\sigma_i^2}$$

The error $\sigma_{\Delta E}$ is obtained from the signal Monte Carlo samples. For the $\mu^+\mu^-$ modes the mean of the ΔE distribution is typically zero, while for the e^+e^- modes due to decay radiation it is shifted to negative values E_0. The dE/dx and TOF weights (if present) are determined for each charged hadron in the final state under study. In each channel all resonance mass constraints are considered. The resolutions are obtained from the MC signal modes. The combination with the smallest χ^2 per degree of freedom is selected in each mode.

To select signal candidates we define signal windows by $\pm 2.5\sigma_{m_B}$ and $E_0 - 2.5\sigma_{\Delta E}, E_0 + 2.5\sigma_{\Delta E}$. The resolutions of the beam-constrained mass are typically 2.4 MeV/c^2, whereas the ΔE resolutions range from 21 MeV to 27 MeV. For background determination we also define a grand side band by $\mid \Delta E \mid > 3.5\sigma_{\Delta E}$ or $5.18 < m_B < 5.27$ GeV/c^2. To remove the contribution from the long distance processes $B \to J/\psi K^{(\star)}$ and $B \to \psi' K^{(\star)}$, which apart from a $J/\psi(\psi')$ mass peak look just like the signal from the electroweak penguin decays, we define J/ψ and ψ' mass windows by:

$$-0.15 < (m_{ee} - m_{\psi^{(\prime)}}) < 0.1 \text{ GeV/c}^2$$

and

$$-0.1 < (m_{\mu\mu} - m_{\psi^{(\prime)}}) < 0.05. \text{ GeV/c}^2$$

The mass windows are asymmetric in order to account for decay radiation of the final state leptons. Signal candidates are required to have dilepton masses which lie outside the J/ψ and ψ' mass windows.

III. BACKGROUND ESTIMATE

Besides leakage from $B \to J/\psi K^{(*)}$ and $B \to \psi' K^{(*)}$ final states, background can originate from modes with two semileptonic decays producing opposite-sign leptons, events with a high-energy photon conversion or a π^0 Dalitz decay, or from single semileptonic decays with a hadron misidentified as a lepton. These processes can originate both from $B\bar{B}$ and $q\bar{q}$ continuum events. To eliminate background from Dalitz pairs and photon conversions we require that $m_{ee} > 0.06$ GeV/c^2 after extrapolating the electrons to the decay vertex. The residual background is determined from high statistics Monte Carlo samples as well as the data grand side band.

The first study involved high statistics $B\bar{B}$ and $q\bar{q}$ continuum samples, which were generated with a fast parametrized Monte Carlo. These MC samples are respectively factors of 27.5 and 39.6 larger than the data sample. The second study involved a detailed $B\bar{B}$ Monte Carlo simulation based on GEANT for both semileptonic B decays and semileptonic $b \to c$ cascade decays. Both samples are a factor of 6.2 larger than the data sample. A third study was performed on the continuum data sample and on the grand side band of the data sample. The overall background estimates from the full Monte Carlo samples and the data grand side bands are summarized in Table II in column three.

IV. EFFICIENCY

To determine the efficiencies we have generated samples of 10^4 events for each of the $e^+e^-K^+(K^0_S)$ and $\mu^+\mu^-K^+(K^0_S)$ modes and 2×10^4 events for each of the $e^+e^-K^\star$ and $\mu^+\mu^-K^\star$ modes, using the Greub-Wyler model [10]. The resulting efficiencies including the branching fractions for K^0_s and K^* decays to their final states are summarized in TableII in column four.

The efficiencies of the $\mu^+\mu^-$ modes are $\sim 20\%$ smaller than those in the e^+e^- modes. This is basically caused by a 1 GeV/c μ momentum cut-off. The highest efficiencies are obtained for the $\mu\mu K^+$ and eeK^+ modes yielding 17% and 23%, respectively. For the $\mu^+\mu^- K^0_S$ and $e^+e^- K^0_S$ modes the acceptances are reduced by about a factor of two with respect to the corresponding charged modes. This is caused by reconstructing a fourth charged track and by imposing a K^0_S mass constraint. Similarly, $\mu^+\mu^- K^+\pi^-$ and $e^+e^- K^+\pi^-$ modes have an additional track plus a K^* invariant mass constraint. Thus, their acceptances are close to those in the corresponding $l^+l^- K^0_S$ modes. Replacing a π^+ by a π^0 or adding in more charged tracks yields further efficiency reductions.

V. RESULTS

The $\Delta E - m_B$ correlation for the samples after J/ψ and ψ' removal are displayed in Figures 3 and 4. In the signal regions of the dimuon modes we find 2 candidates in the $\mu^+\mu^- K^+$ final state and 1 candidate in the $\mu^+\mu^- K^+\pi^0$ final state. In the signal region of the dielectron modes we observe 4 candidates in the $e^+e^- K^+$ final state, and 1 candidate each in the $e^+e^- K^+\pi^0$ and $e^+e^- K^+\pi^-$ final states. The observed yields are consistent with background. For the $e^+e^- K^+$ mode the probability that the expected background fluctuates up to four is 0.34%. The observed yields are summarized in Table II in column two.

In order to check our sensitivity for observing $B \to K^{(*)} l^+l^-$ modes we have studied the color-suppressed decays $B \to J/\psi K^{(*)}$ with $J/\psi \to l^+l^-$ using the same selection criteria. The m_{ll} mass spectra for events inside the $\Delta E - M_B$ signal region are shown in Figures 5 and 6. In the dominant final states $K^+l^+l^-$, $K^0_S l^+l^-$, $K^+\pi^- l^+l^-$, and $K^+\pi^0 l^+l^-$, J/ψ and ψ' signals are clearly visible. We determine branching fractions which are in good agreement with previously published values [21], demonstrating the capability to observe these FCNC decays.

The branching fraction upper limits at 90% confidence level (CL) are determined with a Poissonian probability distribution by considering the number of observed events as signal. Taking a conservative approach the estimated background is not taken into account. Counting all candidates as signal we determine branching fraction upper limits at a 90% confidence level (CL) summarized in column five of Table II. These limits do not include systematic errors, which range from 8-14% depending on the mode. The systematic error determination is discussed in the next section. The branching fraction upper limits at 90% CL including systematic errors are listed in column six of Table II.

The best individual upper limits are obtained for $B \to \mu^+\mu^- K^{*0}$ and $B \to \mu^+\mu^- K^+$ modes:

$$\mathcal{B}(B \to \mu^+\mu^- K^{*0}) < 0.95 \times 10^{-5} \quad \text{at} \quad 90\% \text{ CL}$$

$$\mathcal{B}(B \to \mu^+\mu^- K^{+}) < 0.97 \times 10^{-5} \quad \text{at} \quad 90\% \text{ CL}$$

For the corresponding e^+e^- modes we determine:

TABLE II. Yields, estimated background, total efficiencies, and branching fraction upper limits at 90% CL without and with systematic errors

mode	yield [events]	estimated background [events]	ϵ_{tot} [%]	B (no sys) $[10^{-5}]$	B with (sys) $[10^{-5}]$
$\mu^+\mu^-K^+$	2	0.7 ± 0.2	17.2 ± 0.4	< 0.93	< 0.97
$\mu^+\mu^-K^0$	0	0.2 ± 0.1	3.6 ± 0.1	< 1.9	< 2.1
$\mu^+\mu^-K^{*+}$	1	1.5 ± 0.2	3.9 ± 0.2	< 3.0	< 3.3
$\mu^+\mu^-K^{*0}$	0	1.3 ± 0.2	7.9 ± 0.3	< 0.87	< 0.95
$e^+e^-K^+$	4	0.6 ± 0.2	23.0 ± 0.5	< 1.0	< 1.1
$e^+e^-K^0$	0	0.1 ± 0.1	4.7 ± 0.1	< 1.5	< 1.7
$e^+e^-K^{*+}$	1	1.8 ± 0.2	4.5 ± 0.2	< 2.6	< 2.8
$e^+e^-K^{*0}$	1	2.1 ± 0.2	9.3 ± 0.2	< 1.3	< 1.4

$$\mathcal{B}(B \to e^+e^-K^{*0}) < 1.4 \times 10^{-5} \quad \text{at} \quad 90\% \text{ CL}$$

$$\mathcal{B}(B \to e^+e^-K^+) < 1.1 \times 10^{-5} \quad \text{at} \quad 90\% \text{ CL}$$

These values are based on the conservative upper limit determination without accounting for the background and include the systematic uncertainties.

We can proceed further and average charged and neutral B decay channels. We find improved limits for the $B \to l^+l^-K$ modes:

$$\mathcal{B}(B \to \mu^+\mu^-K) < 0.83 \times 10^{-5} \quad \text{at} \quad 90\% \text{ CL}$$

$$\mathcal{B}(B \to e^+e^-K) < 0.94 \times 10^{-5} \quad \text{at} \quad 90\% \text{ CL}$$

Combining the charged and neutral $l^+l^-K^*$ modes only yields a minor improvement for the $e^+e^-K^*$ channel:

$$\mathcal{B}(B \to \mu^+\mu^-K^*) < 1.1 \times 10^{-5} \quad \text{at} \quad 90\% \text{ CL}$$

$$\mathcal{B}(B \to e^+e^-K^*) < 1.3 \times 10^{-5} \quad \text{at} \quad 90\% \text{ CL}$$

Note that all these limits are higher than the Standard Model predictions.

From the $b \to s\gamma$ branching fraction measurement we can estimate the contributions of new physics affecting the Wilson coefficient $C_7^{(0)eff}$. To increase the sensitivity for new physics contributions in the Wilson coefficients C_9^{eff} and C_{10} we average both e^+e^-K and $\mu^+\mu^-K$ final states. In the Kl^+l^- modes there is no singularity for $m_{ll} \to \infty$. The effect from $C_7^{(0)eff}$ in the entire mass region is just 6%. The branching fraction upper limit for the combined l^+l^-K modes is:

$$\mathcal{B}(B \to l^+l^-K) < 0.70 \times 10^{-5} \quad \text{at} \quad 90\% \text{ CL}$$

This is still about a factor of five above the SM prediction for the combined Kl^+l^- mode.

TABLE III. Systematic Uncertainties

mode	$B\bar{B}$ prod. [%]	Lepton ID [%]	K ID [%]	Tracking [%]	π^0 Finding [%]	ϵ [%]	Total Sys. Error [%]
$\mu^+\mu^-K^+$	1.8	2.0	3.0	6.0	-	2.1	7.5
$\mu^+\mu^-K^0_S(\pi^+\pi^-)$	1.8	2.0	3.0	8.0	-	2.9	9.4
$\mu^+\mu^-K^{*+}(K^+\pi^0)$	1.8	2.0	3.0	6.0	2.0	4.7	8.9
$\mu^+\mu^-K^{*+}(K^0_S\pi^+)$	1.8	2.0	3.0	10.0	-	6.7	12.7
$\mu^+\mu^-K^{*0}(K^+\pi^-)$	1.8	2.0	3.0	8.0	-	2.6	9.3
$\mu^+\mu^-K^{*0}(K^0_S\pi^0)$	1.8	2.0	3.0	8.0	2.0	10.0	13.6
$e^+e^-K^+$	1.8	2.0	3.0	6.0	-	2.3	7.6
$e^+e^-K^0_S(\pi^+\pi^-)$	1.8	2.0	3.0	8.0	-	3.5	9.6
$e^+e^-K^{*+}(K^+\pi^0)$	1.8	2.0	3.0	6.0	2.0	4.5	8.7
$e^+e^-K^{*+}(K^0_S\pi^+)$	1.8	2.0	3.0	10.0	-	6.6	12.6
$e^+e^-K^{*0}(K^+\pi^-)$	1.8	2.0	3.0	8.0	-	2.7	9.4
$e^+e^-K^{*0}(K^0_S\pi^0)$	1.8	2.0	3.0	8.0	2.0	9.5	13.2

In the case of $K^*l^+l^-$ modes we encounter a singularity for zero dilepton masses that is due to the influence of $B \to K^*\gamma$ and affects only the Wilson coefficient $C_7^{(0)eff}$. To reduce the effect of $C_7^{(0)eff}$ to less than 16%, we reject events with dilepton masses below 0.5 GeV/c^2 and redo the analysis using the Fisher discriminant obtained for Kl^+l^- modes. We keep all other selection criteria the same as before. The observed yield is now two events and the estimated background corresponds to 5.7 ± 0.4 events. This leads to a branching fraction upper limit for the combined $l^+l^-K^*$ mode of:

$$\mathcal{B}(B \to l^+l^-K^*) < 0.68 \times 10^{-5} \quad \text{at} \quad 90\% \text{ CL}$$

These upper limits also lie above the SM predictions, approaching the predictions of the Ali-Mannel model. Figure 7 shows our branching fraction upper limits in comparison to the range of SM predictions and previous limits.

We do not observe any significantly large component of $B \to K^*l^+l^-$ modes. This indicates that new physics contributions in the Wilson coefficients $C_9^{eff}(\mu)$ and $C_{10}(\mu)$ are not extraordinarily large.

VI. SYSTEMATIC UNCERTAINTIES

The individual contributions of systematic errors are listed in Table III. The knowledge of $B\bar{B}$ production at the $\Upsilon(4S)$ is accurate to 1.8%. The uncertainty for identifying electrons and muons is typically 2% each. The requirement for a charged track to be consistent with a K at the 3σ level is about 3%. One of the largest errors is due to uncertainties in tracking.

For $B\bar{B}$ events the uncertainty is about 2% per track. For each final state the errors for all tracks per final state are added linearly. The systematic error for π^0 detection is about 2%. Another systematic error contribution comes from the efficiency determination, which is dominated by the Monte Carlo statistics. For the dominant final states the efficiency determination is accurate to $2-5\%$. For the suppressed final states the efficiencies are precise within $7-10\%$. Thus, the dominant systematic errors are tracking, and for some final states, Monte Carlo statistics. The overall systematic errors are obtained by adding all individual contributions in quadrature. The systematic errors range from 8% to 10% for the dominant $l^+l^-K^{(*)}$ final states and about 13% for the suppressed $l^+l^-K^*$ final states.

VII. CONCLUSION

We have searched for electromagnetic penguin decays of B mesons with a K or a K^* and two oppositely charged leptons in the final state. One of the best branching fraction upper limits is obtained for the $\mu^+\mu^-K^+$ mode yielding $\mathcal{B}(B \to \mu^+\mu^-K^+) < 0.97 \times 10^{-5}$ at 90% CL. This is more than an order of magnitude above the SM predictions. The corresponding dielectron branching fraction upper limit is $\mathcal{B}(B \to e^+e^-K^+) < 1.1 \times 10^{-5}$ at 90% CL.

The $e^+e^-K^{*0}$ mode individually provides the highest sensitivity for testing the Standard Model, since the predicted branching fraction is the highest among the exclusive l^+l^-K and $l^+l^-K^*$ modes and is experimentally easily accessible achieving a high efficiency for a low background level. The observed branching fraction upper limit is $\mathcal{B}(B \to e^+e^-K^{*0}) < 1.3 \times 10^{-5}$ at 90% CL. In the corresponding dimuon mode we obtain $\mathcal{B}(B \to \mu^+\mu^-K^{*0}) < 0.95 \times 10^{-5}$ at 90% CL. Combining the $\mu^+\mu^-$ and e^+e^- final states yields branching fraction upper limits of $\mathcal{B}(B \to l^+l^-K) < 0.7 \times 10^{-5}$ at 90% CL and $\mathcal{B}(B \to l^+l^-K^*) < 0.68 \times 10^{-5}$ at 90% CL. For the latter mode only dilepton masses above 0.5 GeV/c^2 were considered in order to reduce effects from the Wilson coefficient $C_7^{(0)eff}(\mu)$.

Our branching fraction upper limits are the lowest ones and provide for most modes considerable improvements over present results [22], [17], [18]. However, all of them still lie above the SM predictions [10], [11], [7], [12]. The absence of a signal in the $K^*l^+l^-$ modes indicates that there are no extremely large contributions from processes beyond the Standard Model, which would enhance the $B \to K^*l^+l^-$ rate. In order to pin down new physics contributions, a significant increase in statistics is needed. With the expected factor of 5 increase in luminosity at CESR this may be achieved within the next 5 years in CLEO III.

VIII. ACKNOWLEDGMENTS

We gratefully acknowledge the effort of the CESR staff in providing us with excellent luminosity and running conditions. This work was supported by the National Science Foundation, the U.S. Dept. of Energy, the Natural Science and Engineering Research Council of Canada, and the A.P. Sloan Foundation.

REFERENCES

[1] N. G. Deshpande, K. Panose, and J. Trampetic, Phys. Lett **B308**, 3222 (1993).

[2] Y. Grossman, Nucl. Phys. **B426**, 355 (1995).

[3] P. Cho, M. Misiak and D. Wyler, Phys. Rev. **D54**, 3329 (1996).

[4] K. Peterson, Phys. Lett. **B282**, 207 (1992).

[5] A. J. Buras and R. Fleischer, preprint TUM-HEP-275-97, 174pp (1997); G. Buchalla, A. J. Buras and M. E. Lautenbacher, Rev.Mod.Phys. **68**, 1125 (1996) and references therein.

[6] M. Gourdin, Phys. Lett. **B316**, 578 (1993); P.J. O'Donnel, M. Sutherland and H.K.K. Tung, Phys. Rev. **D46**, 4091 (1992); B. Grinstein, M.J. Savage, and M.B. Wise, Nucl. Phys. **B319**, 271 (1989); N.G. Deshpande and J. Trampetic, Phys. Rev. Lett. **60**, 2583 (1988); W.S. Hou, R.S. Willey, and A. Soni, Phys. rev. Lett. **58**, 1608 (1987); R. Grigjanis, P.J. O'Donnel, M.Sutherland, and H. Navelet, Phys. Lett. B 223, 239 (1989); G. Eilam *et al.,* Phys. Rev. **D34**, 2773 (1986; G. Eilam *et al.,* Phys. Rev. Lett. **57**, 1106 (1986).

[7] A. Ali and T. Mannel, Phys. Lett. **B264**, 447 (1991); A. Ali, Nucl. Instrum. Meth. **A384**, 8 (1996).

[8] A. Ali, T. Mannel and T. Morozumi, Phys.Lett. **B273** 505 (1991).

[9] A. Ali, G.F. Giudice, T. Mannel, Z.Phys. **C67** 417 (1995).

[10] C. Greub, A Ioannisian and D. Wyler, Phys. Lett. **B346** 149 (1994).

[11] P. Ball and V.M. Braun, CERN-TH-98-162, 36pp (1998).

[12] D. Melikhov and N. Nikitin, hep-ph/9609503, 8pp (1996).

[13] A.J. Buras and M. Münz, Phys. Rev. **D52**, 186 (1995).

[14] R. Ammar *et al.,* CLEO collaboration, Phys. Rev. Lett. **71**, 674 (1993).

[15] S. Alam *et al.,* CLEO collaboration, Phys. Rev. Lett. **74**, 2885 (1995).

[16] S. Glenn *et al.,* CLEO collaboration, Phys. Rev. Lett. **80**, 2289 (1997).

[17] R. Balest *et al.,* CLEO collaboration, CLEO-CONF-94-4 submitted to ICHEP Glasgow, 16pp (1994).

[18] F. Abe *et al.,* CDF collaboration, Phys. Rev. Lett. **76**, 4675 (1996).

[19] Y. Kubota *et al.,* CLEO collaboration, Nucl. Instr. Meth. **A320**, 66 (1992).

[20] C.H. Wang, PhD Thesis, Univ. of Rochester (1993); M. Battle, PhD Thesis, Univ. of Rochester (1994).

[21] C.P. Jessop *et al.,* CLEO collaboration, Phys. Rev. Lett **79**, 4533 (1997).

[22] R.M. Barnett *et al.,* (Particle Data Group), Phys. rev. **D54**, 1 (1996).

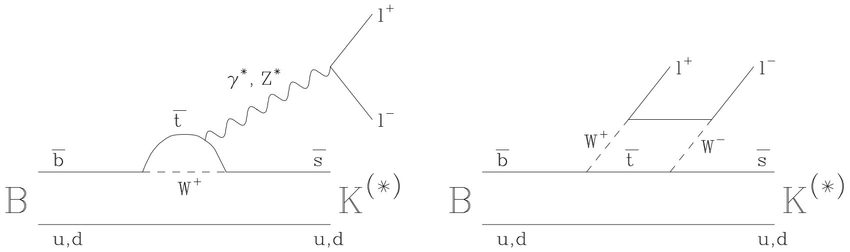

FIG. 1. Lowest order Feynman diagrams for $B \to K l^+ l^-$ and $B \to K^* l^+ l^-$ modes.

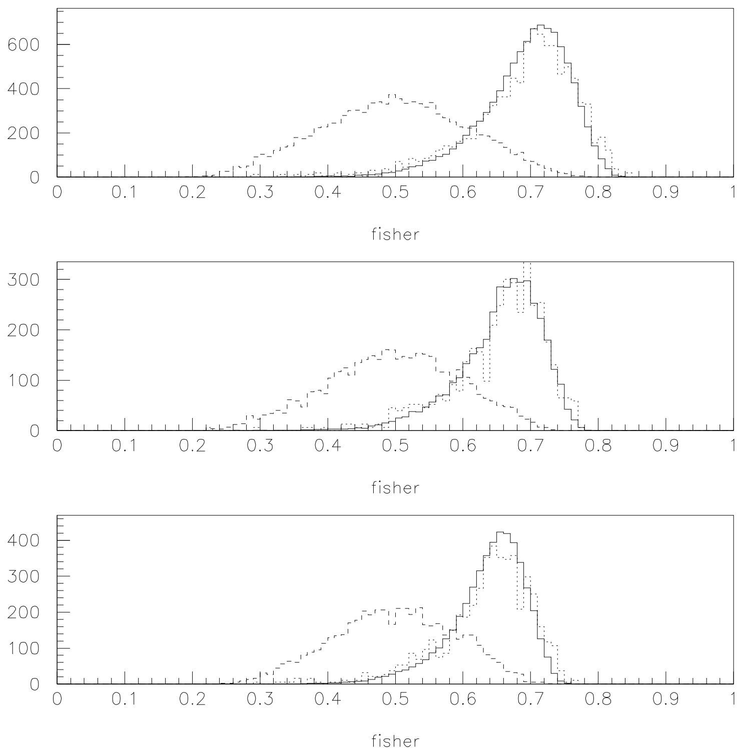

FIG. 2. Fisher discriminants of signal modes (dashed curve), $q\bar{q}$ continuum from Monte Carlo (solid curve) and $q\bar{q}$ continuum from data (dotted) curve for a) $B \to K l^+ l^-$ modes, b) $B \to K^* \mu^+ \mu^-$ modes, and c) $B \to K^* e^+ e^-$ modes (from top to bottom).

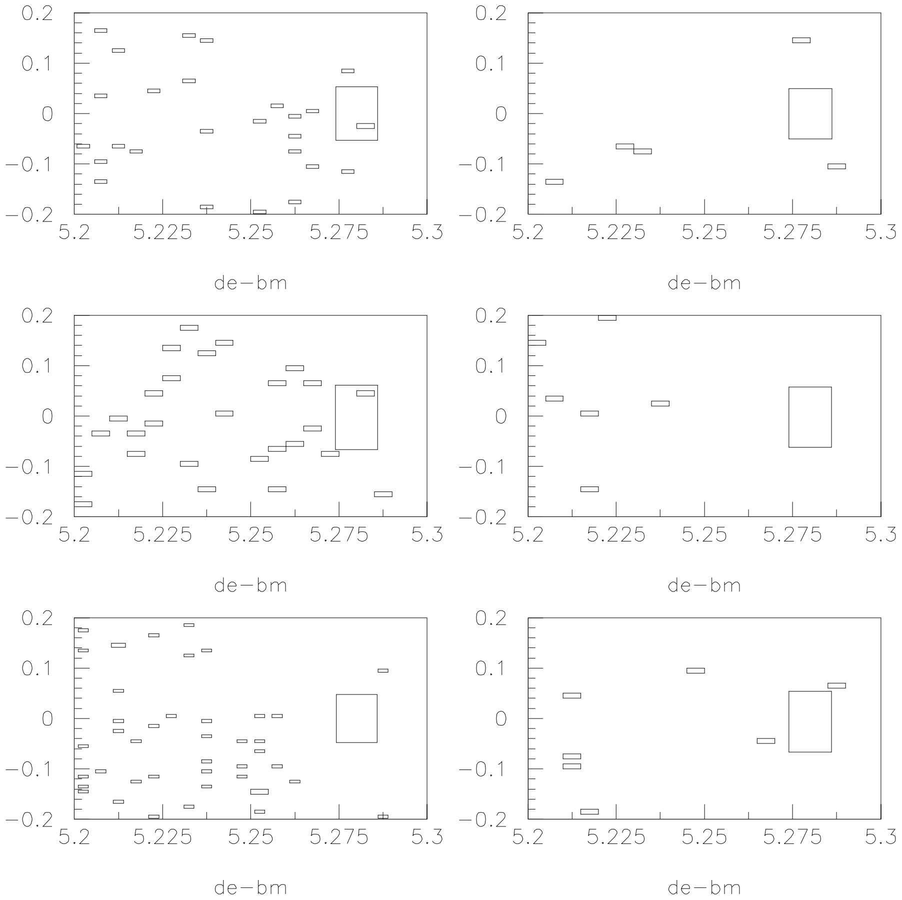

FIG. 3. $\Delta E - m_b$ correlations after removal of J/ψ and ψ' events for: a) $B^+ \to K^+\mu^+\mu^-$, b) $B^0 \to K^0_S\mu^+\mu^-$ $(\pi^+\pi^-)$, c) $B^+ \to K^{*+}\mu^+\mu^-$ $(K^+\pi^0)$, d) $B^+ \to K^{*+}\mu^+\mu^-$ $(K^0_S\pi^+)$, e) $B^0 \to K^{*0}\mu^+\mu^-$ $(K^+\pi^-)$, f) $B^+ \to K^{*0}\mu^+\mu^-$ $(K^0_S\pi^0)$ (from left to right, top to bottom.

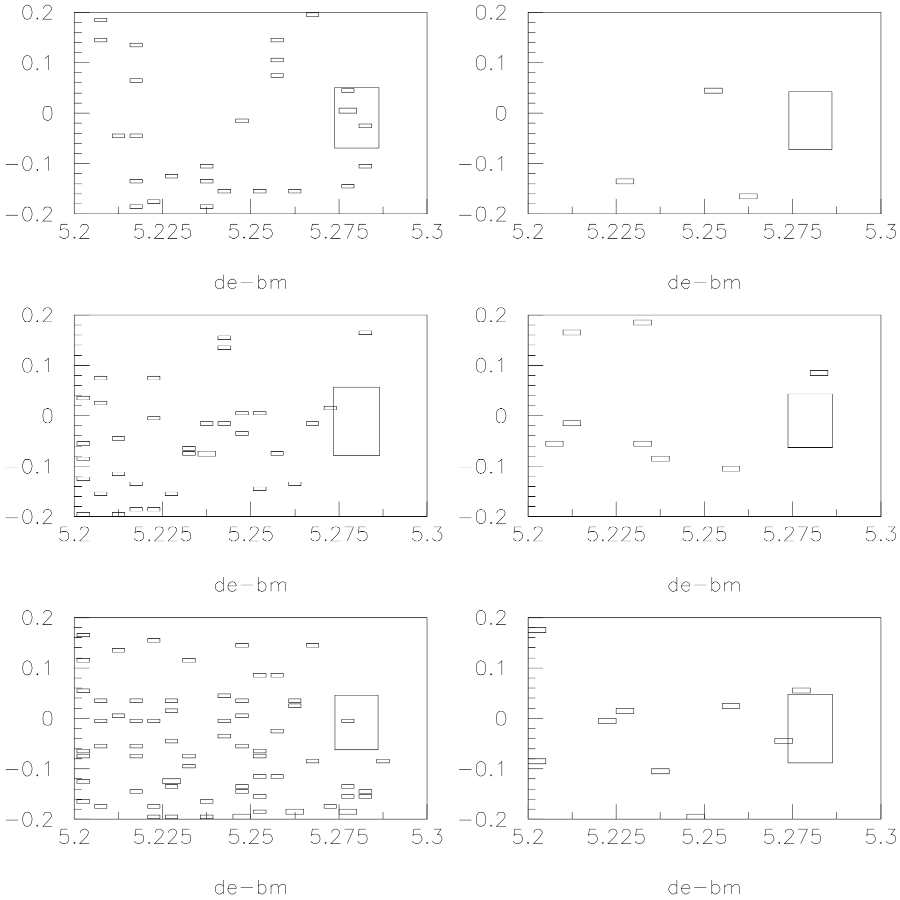

FIG. 4. $\Delta E - m_b$ correlations after removal of J/ψ and ψ' events for: a) $B^+ \to K^+e^+e^-$, b) $B^0 \to K^0_S e^+e^-$ $(\pi^+\pi^-)$, c) $B^+ \to K^{*+}e^+e^-$ $(K^+\pi^0)$, d) $B^+ \to K^{*+}e^+e^-$ $(K^0_S\pi^+)$, e) $B^0 \to K^{*0}e^+e^-$ $(K^+\pi^-)$, f) $B^+ \to K^{*0}e^+e^-$ $(K^0_S\pi^0)$ (from left to right, top to bottom).

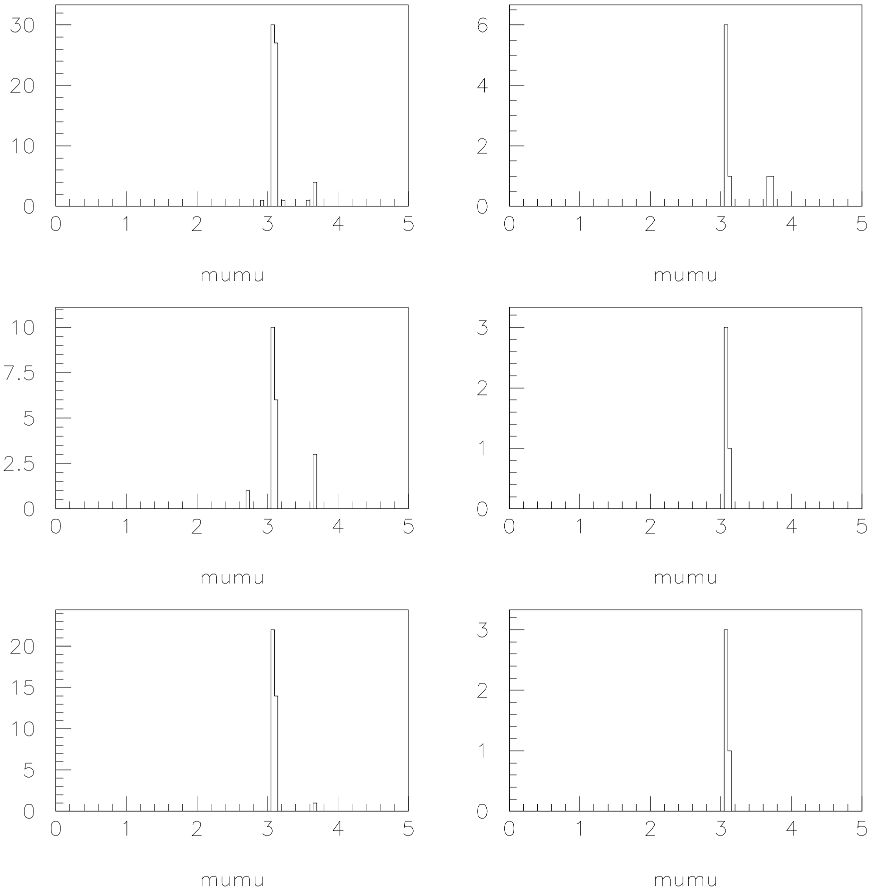

FIG. 5. Dimuon mass spectrum before removal of J/ψ and ψ' events for: a) $B^+ \to K^+\mu^+\mu^-$, b) $B^0 \to K_S^0\mu^+\mu^-$ $(\pi^+\pi^-)$, c) $B^+ \to K^{*+}\mu^+\mu^-$ $(K^+\pi^0)$, d) $B^+ \to K^{*+}\mu^+\mu^-$ $(K_S^0\pi^+)$, e) $B^0 \to K^{*0}\mu^+\mu^-$ $(K^+\pi^-)$, f) $B^+ \to K^{*0}\mu^+\mu^-$ $(K_S^0\pi^0)$ (from left to right, top to bottom).

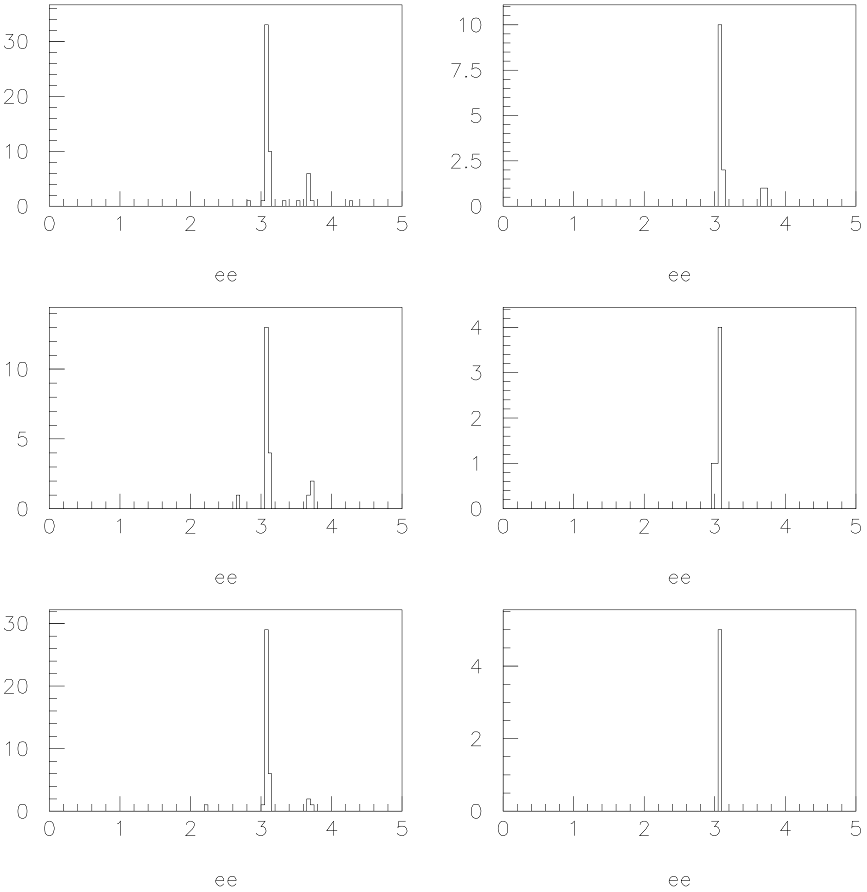

FIG. 6. Dielectron mass spectrum before removal of J/ψ and ψ' events for: a) $B^+ \to K^+e^+e^-$, b) $B^0 \to K^0_S e^+e^-$ $(\pi^+\pi^-)$, c) $B^+ \to K^{*+}e^+e^-$ $(K^+\pi^0)$, d) $B^+ \to K^{*+}e^+e^-$ $(K^0_S\pi^+)$, e) $B^0 \to K^{*0}e^+e^-$ $(K^+\pi^-)$, f) $B^+ \to K^{*0}e^+e^-$ $(K^0_S\pi^0)$ (from left to right, top to bottom).

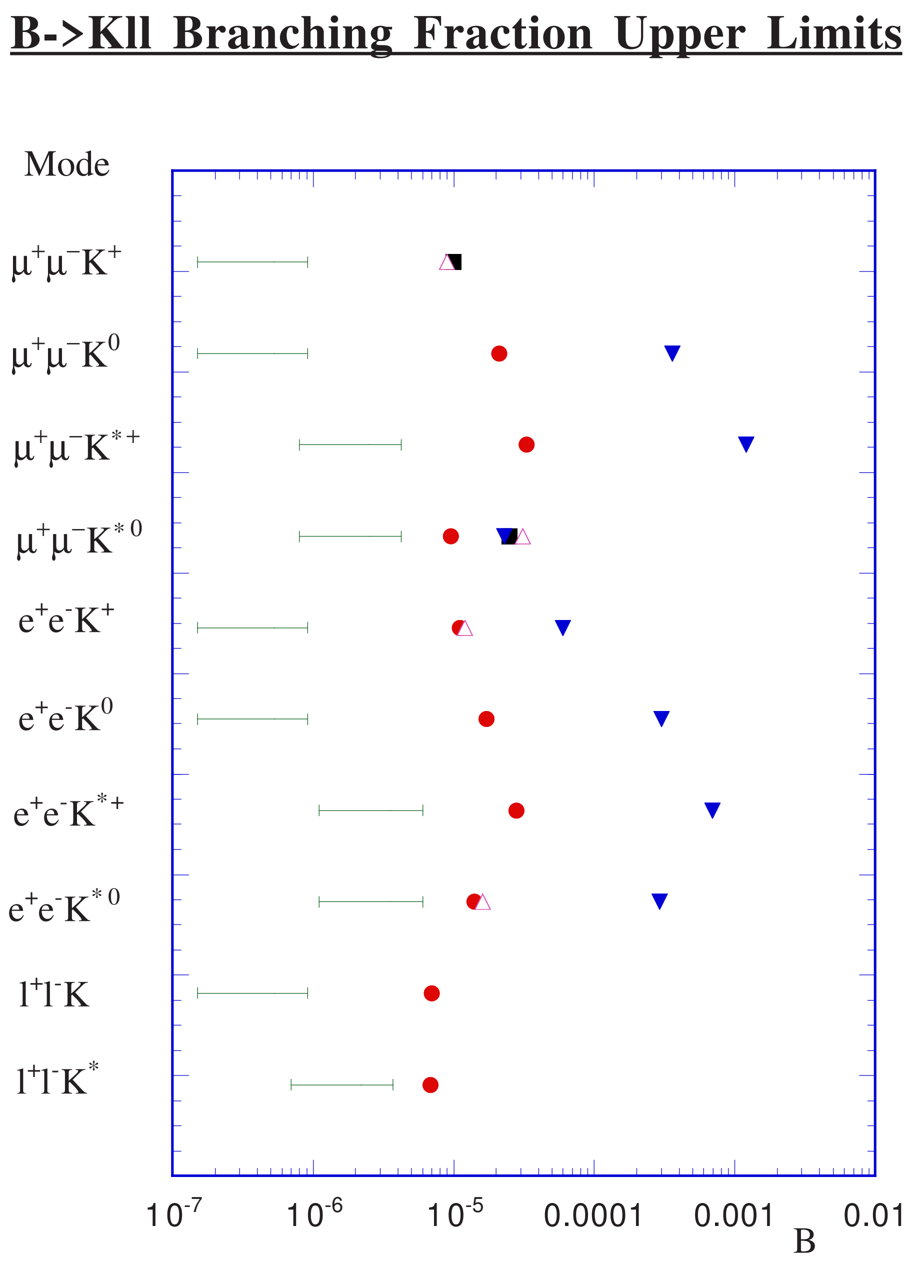

FIG. 7. Comparison of all branching fraction upper limits at 90% CL of SM prediction (solid lines), present analysis (solid circles), status in 1995 (downward triangles) [17], previously published results (upward triangles) [22] and recent CDF results (solid squares) [18].